

# MicroRNA-126 modulates the tumor microenvironment by targeting calmodulin-regulated spectrin-associated protein 1 (Camsap1)

XIN SUN<sup>1</sup>, ZHI-MING WANG<sup>2</sup>, YAN SONG<sup>1</sup>, XU-HUI TAI<sup>4</sup>, WEN-YUE JI<sup>1</sup> and HUI GU<sup>3</sup>

Departments of <sup>1</sup>Otorhinolaryngology and <sup>2</sup>Stomatology, <sup>3</sup>Central Laboratory, Shengjing Hospital, China Medical University, Shenyang 110004; <sup>4</sup>Department of Otorhinolaryngology, Chinese PLA 463 Hospital, P.R. China

Received December 29, 2013; Accepted February 14, 2014

DOI: 10.3892/ijo.2014.2321

**Abstract.** Plasma miRNAs have been reported as biomarkers for various diseases. In this study, we investigated whether plasma concentrations of miR-126 may be useful as biomarkers for laryngeal squamous cell carcinoma (LSCC). We examined the function and mechanism of miR-126 in LSCC by using cell biology and molecular pathology techniques such as western blotting, quantitative PCR, IHC and IF. The expression of Camsap1 mRNA and protein is higher in cancer tissues compared to that in normal tissues. Both miR-126 and Camsap1 were related with the prognosis of LSCC patients. We found that miR-126 was able to inhibit LSCC partly by suppressing Camsap1 expression. In addition, Camsap1 expression induced microtubule formation and aggregation. This mechanism possibly explains why loss of miR-126 is frequently associated with tumor metastasis.

## Introduction

MicroRNAs (miRNAs) are short, non-coding RNA molecules that post-transcriptionally regulate the expression of target genes, and play a role in diverse cellular, physiological and pathophysiological processes (1-3). MicroRNA-126 (miR-126) is located within intron 7 of epidermal growth factor-like domain 7 (EGFL7) and is highly expressed in vascular endothelial cells (4,5). To date, it has been reported that the miR-126 expression differs between normal tissues and derived tumors (6-8). miR-126 is also strongly downregulated in pancreatic cancer, with an associated elevation in K-Ras (9), and lower expression of miR-126 is significantly correlated with short survival in non-small cell lung carcinoma (NSCLC)

and renal cell carcinoma (10). Recent studies have shown that some miRNAs are present in the systemic circulation and are associated with exosomes and microparticles (11,12). The levels of some circulating miRNAs have been reported to be differentially expressed in the presence of a variety of cancers (13,14).

However, to our knowledge, no previous study exists showing the relationship between miR-126 and laryngeal squamous cell carcinoma (LSCC). In this study, we assessed the levels of circulating miR-126 in serum of the patients with LSCC. In addition, we focused on a target protein of miR-126, Camsap1. We also investigated the function and mechanism of miR-126 and Camsap1 in the LSCC cells. This study provides new insights into the potential mechanisms of LSCC oncogenesis and metastasis.

## Materials and methods

**Sample collection.** After obtaining Our University Ethics Committee approval and informed consent from all study participants, tissue samples and blood samples were drawn at the Department of Otorhinolaryngology, Shengjing Hospital, China Medical University in 2010 and 2011. Up to 8 ml of whole blood were collected from each participant in an ethylene diamine tetracetic acid tube. Blood samples were centrifuged at 1,200 x g for 10 min at 4°C to separate the blood cells, and the supernatant was transferred into microcentrifuge tubes and then centrifuged a second time at 12,000 x g for 10 min at 4°C to completely remove the cellular components. Plasma was aliquoted and stored at -80°C until use. Blood samples were processed and plasma was frozen within 4 h of collection.

**Real-time PCR.** Total RNA (2 µg) was reverse-transcribed using Transcript First-strand cDNA Synthesis SuperMix (TransGen Biotech, Beijing, China) according to the manufacturer's protocol. In short, the 50 µl reactions were incubated for 60 min at 42°C, 10 min at 70°C, and then stored at 4°C. qRT-PCR analyses were performed using the Bulge-Loop™ miRNA qRT-PCR Detection kit (Ribobio Co., Guangzhou, China) and TransStart™ Green qPCR SuperMix (TransGen Biotech) according to with the manufacturer's protocol with

*Correspondence to:* Dr Wen-Yue Ji, Department of Otorhinolaryngology, Shengjing Hospital, China Medical University, Shenyang 110001, P.R. China

E-mail: ji\_wenyue2004@163.com

**Key words:** laryngeal carcinoma, miR-126, Camsap1, survival rate, apoptosis

the Rotor-Gene 6000 system (Qiagen, Hilden, Germany). Briefly, the reactions were incubated at 95°C for 30 sec, followed by 40 cycles of 95°C for 30 sec, 60°C for 20 sec, 70°C for 1 sec. The relative expression level for miRNA-126 was computed using the comparative CT method. It is important to note that to control for possible diversity in the amount of starting RNA, miRNA expression was normalized to small nucleolar RNA U6.

**Isolation and enumeration of CTCs.** The CellSearch system (Veridex, Warren, NJ, USA) is the only test sanctioned by the United States Food and Drug Administration for enumeration of CTCs in clinical practice. Blood samples (5 ml) from patients were drawn into CellSave tubes, which were maintained at room temperature and processed within 72 h of collection. CTCs were defined as nucleated epithelial cell adhesion molecule (EpCAM)-positive cells, lacking cluster of differentiation (CD)45 but expressing cytoplasmic cytokeratins 8, 18 and 19. All CTC evaluations were performed by qualified and trained personnel.

**Western blot analysis.** Specimens were lysed using lysis buffer [50 mM Tris-HCl, pH 7.4, 150 mM NaCl, 1% Triton X-100, 0.1% sodium dodecyl sulfate (SDS), 1 mM ethylenediamine-tetraacetic acid (EDTA), 1 mM Na<sub>3</sub>VO<sub>4</sub>, 1 mM NaF, protease inhibitor cocktail]. The extracts were incubated on ice for 20 min, centrifuged at 12,000 x g for 20 min at 4°C and supernatants collected. Protein concentrations were determined using Bradford assay (Bio-Rad, Hercules, CA, USA), and proteins were resolved by 10% Bis-Tris gel electrophoresis, transferred to a nitrocellulose membrane and western blot analysis performed. Anti-Camsap1 and anti-β-actin were purchased from Santa Cruz Biotechnology (Santa Cruz, CA, USA).

**Cell line and culture.** The human laryngeal cancer cell line Hep-2 was purchased from Shanghai Institutes for Biological Sciences, Chinese Academy of Sciences. The cells were cultured in PRMI-1640 supplemented with 10% heat-inactivated fetal bovine serum (FBS) in a humidified cell incubator with an atmosphere of 5% CO<sub>2</sub> at 37°C. Exponentially growing cells were used for experiments.

**Transfection.** Hep-2 cells were transfected with Precursor Molecules mimicking miR-126 (Pre-miR-126) (Applied Biosystems, Foster, CA, USA) or Camsap1 siRNA (sc-92757, Santa Cruz) by using Lipofectamine 2000 (Invitrogen, Carlsbad, CA, USA) according to the manufacturer's instructions.

**Xenograft assays.** All experiments with animals were performed according to the guidelines of the China Medical University Ethics Committee. NU/NU Nude mice (CrI: NU-Foxn1nu) aged 6-8-weeks were purchased from Charles River (Wilmington, MA, USA). Hep-2 cells (3x10<sup>7</sup> in 200 μl) were subcutaneously injected into the axilla of each mouse. After the tumor diameters reached 3-5 mm, the mice were divided randomly into three groups (untreated, miR-126 mimic, Camsap1 knockdown) and received a 100 μl intratumoral injection of PBS, miR-126 mimic, Camsap1 siRNA.

Three injections were administered at 9 a.m., 3 p.m. and 9 p.m. every three days. Tumor growth was then monitored for 30 days. Every five days until the end of the experiment, one mouse from each group was randomly selected to be anesthetized, photographed and sacrificed. For each tumor, measurements were made using calipers, and tumor volumes were calculated as follows: length x width<sup>2</sup> x 0.52. Tumors were subsequently fixed in 4% paraformaldehyde for 24 h, then embedded in paraffin.

**Survival curves.** Additional mice (n=60) were used to establish xenografts to obtain survival curves. Mice with xenografted tumors (as described above) that reached 3-5 mm in diameter were divided into three treatment groups (n=20 for each). Survival was monitored until the experiments were terminated due to heavy tumor burden.

**Quantification of intratumoral microvessels.** For immunohistochemical staining of CD31, endogenous peroxidase activity was blocked in 4-μm tumor sections with 3% hydrogen peroxide for 30 min. Antigen retrieval was performed in citrate buffer (10 mM, pH 6.0) for 30 min at 95°C in a pressure cooker. CD31 antibodies (Sigma-Aldrich, Carlsbad, CA, USA) were incubated with sections at 1:500 overnight at 4°C. Sections were then incubated with a biotinylated secondary antibody for 1 h at RT, followed by incubation with a streptavidin horseradish peroxidase (HRP) complex (Beyotime, Beijing, China) for 60 min at room temperature. Bound antibody was visualized with 3,3'-diaminobenzidine tetrahydrochloride (DAB, Beyotime). Sections were also counterstained with hematoxylin (Beyotime). Microvessel density was detected using the method of Ivkovic-Kapic *et al.* (15). Regions of highest vessel density were located at low magnification (x40), then the number of vessels present were counted at x200 magnification. Three high magnification fields were counted for each tumor section and the mean microvessel density value was recorded for each. Any individual endothelial cells, or endothelial cell cluster, that was clearly separated from adjacent microvessels was counted as a single microvessel.

**miRNA target prediction.** The miRNA targets predicted by TargetScan (<http://www.targetscan.org/>) are based on the presence of conserved 8 mer, 7 mer and 6 mer sites that match the seed region of each miRNA (16).

**Negative staining electron microscopy.** Tubulin was absorbed for 1 min onto glow-discharged formvar- and carbon-coated grids. The samples were stained in 1.5% uranyl acetate for 25 sec. Images were recorded on a FEI Morgagni 268D transmission electron microscope. Tubulin oligomers were imaged at x120,000 magnification resulting in a pixel size of 0.53 nm.

**Immunofluorescence.** Transfected cells were washed with PBS, fixed in 4% paraformaldehyde, permeabilized in 1% Triton X-100 for 5 min, and blocked with 5% bovine serum albumin in PBS containing 0.5% Triton X-100 for 1 h. Camsap1 expression and tubulin expression were detected using anti-Camsap1 (Santa Cruz) antibody and anti-tubulin (Santa Cruz) antibody, respectively. Cells were washed with PBS and incubated with appropriate secondary fluorophore-

Table I. Relationship between miR-126 levels and clinical pathology in LSCC patients.

Clinicopathological features	n	mir-126 high	mir-126 low	$\chi^2$	P-value
Sex				0.07	0.79
Female	12	4	8		
Male	26	6	20		
Age (years)				0.82	0.37
<55	14	2	12		
≥55	24	8	16		
Differentiation				4.68	0.03
Well	8	5	3		
Moderately/poorly	30	5	25		
Lymph node metastasis				0.28	0.60
-	16	3	13		
+	22	7	15		
T classification				1.21	0.27
T1-2	12	2	10		
T3-4	26	8	18		
Clinical stage				1.01	0.31
I-II	15	6	9		
III-IV	23	4	19		

Tumors were divided into 'low' and 'high' mir-200c expression according to the median level.  $\chi^2$  value, Chi-square distribution.

conjugated antibody for 1 h at room temperature. Secondary antibody used for detection of Camsap1 was Alexa Fluor<sup>®</sup> 488 donkey anti-goat IgG (H+L) (Invitrogen) and tubulin was Alexa Fluor<sup>®</sup> 594 rat anti-mouse IgG (H+L) (Invitrogen).

**Phylogenetic analysis.** Thirty-four separate protein sequences of Camsap1 from a wide range of organisms were extracted

from NCBI. An alignment of these sequences was made using Mega 5.0. To determine the phylogenetic relationships of these sequences, we used maximum likelihood (ML), neighbor-joining (NJ), and Bayesian Markov chain Monte Carlo (MCMC) approaches to infer three individual trees.

**Statistical analysis.** All statistical analyses were carried out using SPSS version 17.0 (Statistical Package for the Social Sciences). The experiments were conducted in triplicates. All numerical data are expressed as the means  $\pm$  SD. Differences among the mean values were evaluated using Student's t-test. P-values <0.05 were considered statistically significant.

## Results

**miR-126 levels in plasma and Camsap1 levels in tissue from the patients with LSCC.** Using qRT-PCR assays, we measured the circulating levels of miR-126 in the patients. Based on this result, we analyzed the potential relationship between the circulating levels of miR-126 and the clinicopathological characteristics of the sampled patients. Results are summarized in Table I. No correlation was found with sex, age, lymph node metastasis, T classification and clinical stage ( $P>0.05$ ). However, miR-126 expression was significantly associated with differentiation of LSCC ( $P<0.05$ ). Western blot analysis and real-time PCR analysis were performed in order to determine the levels of Camsap1 protein and mRNA in LSCC specimens. Both Camsap1 protein and mRNA in cancer tissue was significantly higher than that in matched normal tissue ( $P<0.05$ , Fig. 1).

**Correlation of miR-126, Camsap1 and CTCs.** In the present study, we isolated and enumerated the CTCs in patients using the CellSearch<sup>®</sup> system (Fig. 2A). The patients with <10 CTCs showed a higher survival rate when compared with the patients with >10 CTCs ( $P<0.05$ , Fig. 2B). miR-126 expression was closely correlated with the favorable prognosis of the patients with LSCC, whereas Camsap1 expression was correlated with a poor prognosis ( $P<0.05$ , Fig. 2B). The plasma level of miR-126 and the number of CTCs were significantly negatively correlated ( $r=-0.848$ ,  $P<0.01$ ; Fig. 2C). The plasma level of miR-126 was also negatively related with Camsap1 expression

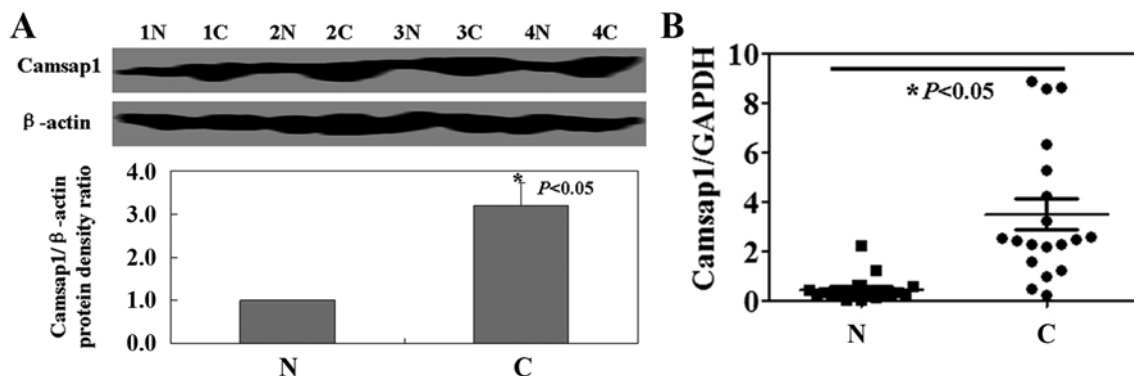


Figure 1. The levels of Camsap1 mRNA and protein in LSCC. (A) Representative results of four paired of LSCC tissues and corresponding normal tissues by western blot analysis.  $\beta$ -actin was used as an internal control. (B) The levels of Camsap1 mRNA were measured in specimens using real-time PCR. GAPDH was used as an internal control. N, normal; C, cancer.

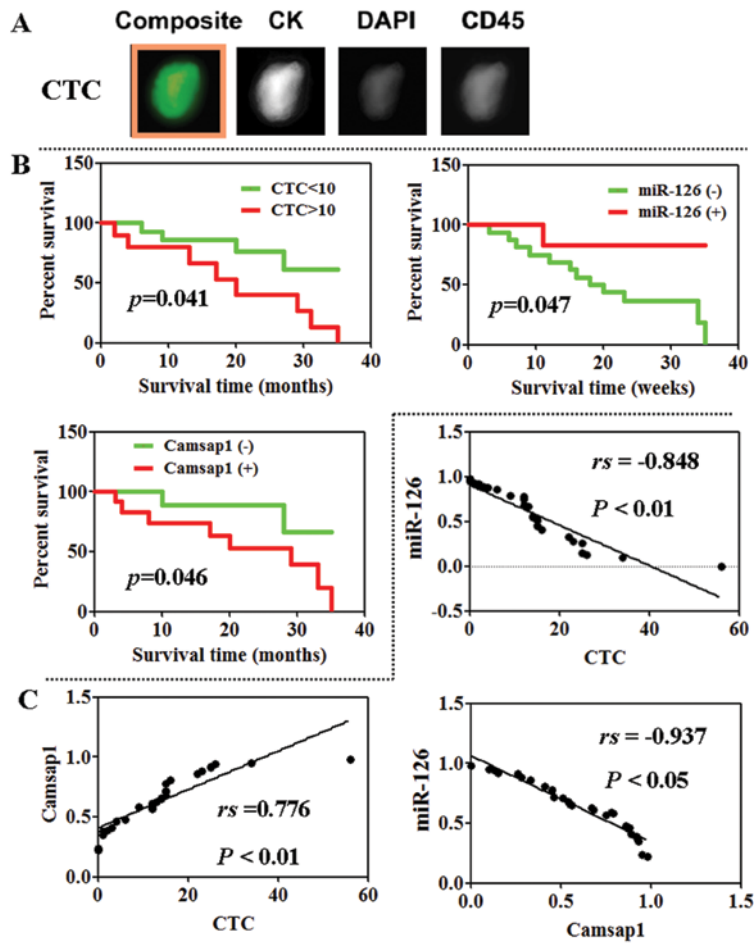


Figure 2. miR-126, Camsap1 and CTCs with the survival rate of the patients with LSCC. (A) CellSearch® images of CTCs from patients with NSCLC. (B) The roles of miR-126, Camsap1 and CTCs in the prognosis of LSCC patients. (C) Correlation among miR-126, Camsap1 and CTCs.

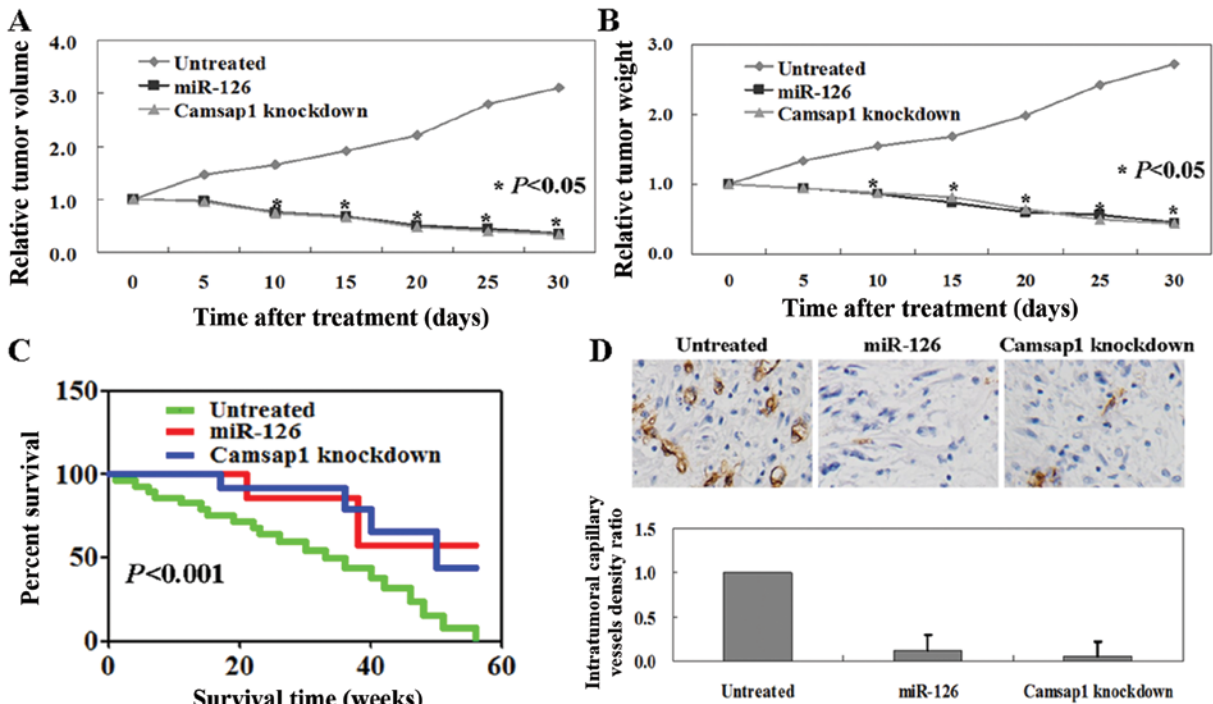


Figure 3. miR-126 mimics or Camsap1 knockdown suppressed tumor growth in xenograft mouse models. (A and B) Tumor volume and tumor weights of the groups described in Materials and methods. (C) Kaplan-Meier survival curves of the groups described in Materials and methods. (D) Immunohistochemical staining of tumor vessel endothelial cells using an anti-CD31 antibody. Bound antibody is detected with DAB and appears brown. Quantitation of vessel density ratios are provided below ± standard deviation.

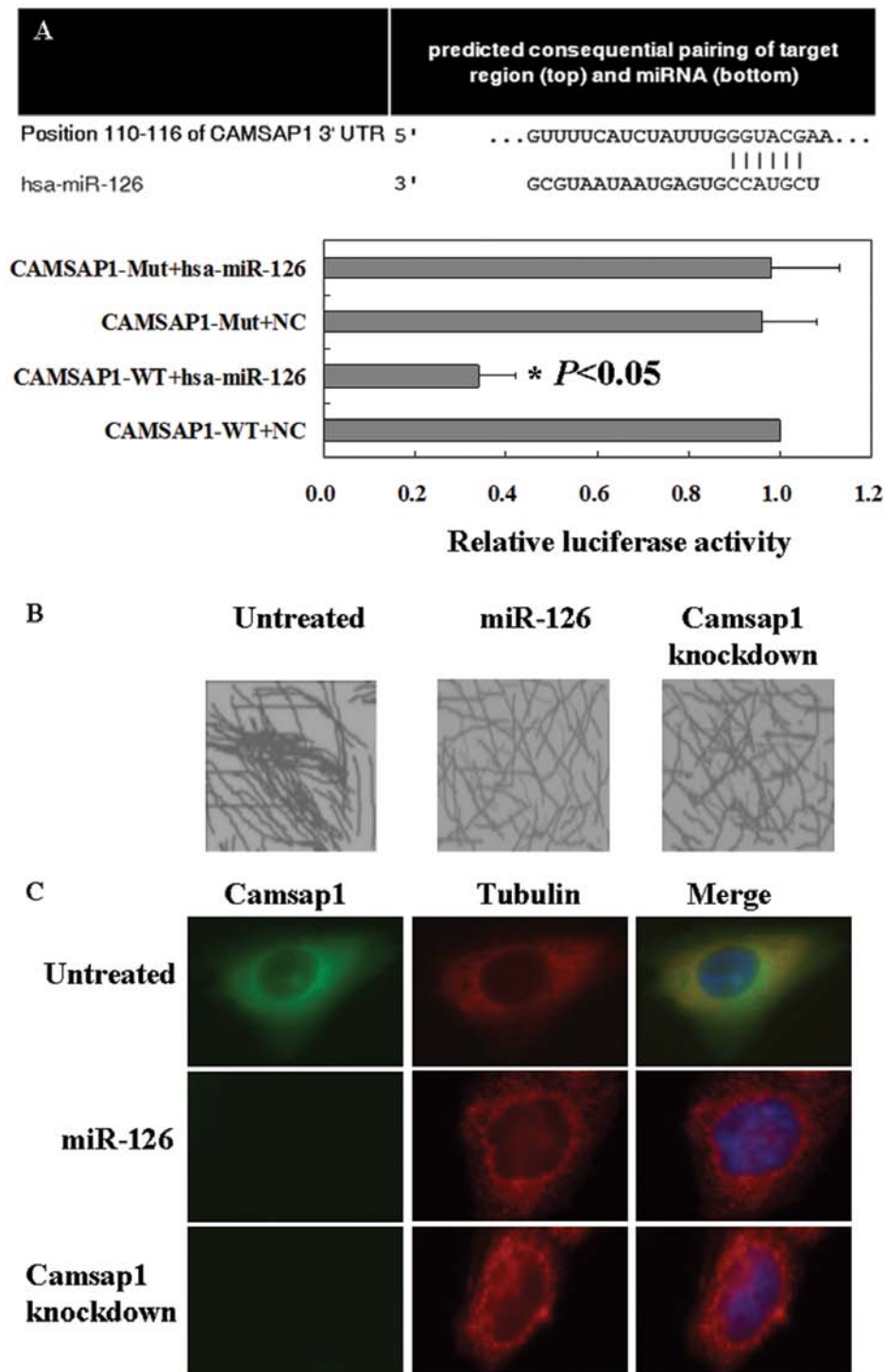


Figure 4. Camsap1 is the target of miR-126. (A) Putative binding sites of miR-126 in the Camsap1. (B) Negative stain electron microscopy of microtubules. (C) Immunofluorescence showed localization of tubulin and Camsap1 in LSCC cells.

( $r = -0.937$ ,  $P < 0.05$ ; Fig. 2C). However, Camsap1 expression was positively related with the number of CTCs ( $r = -0.776$ ,  $P < 0.01$ ; Fig. 2C).

*The roles of miR-126 and Camsap1 in LSCC mouse model.* The antitumor properties of miR-126 and Camsap1 were further evaluated using LSCC mouse models. As shown in Fig. 3A, compared to untreated mice, both miR-126 mimics and Camsap1 knockdown mice had a significant lower tumor

volume ( $P < 0.05$ ). Correspondingly, the tumor weights of miR-126 mimics or Camsap1 knockdown mice also were lower than that of untreated ones ( $P < 0.05$ , Fig. 3B). In addition, the survival rate of mice with miR-126 mimics and Camsap1 knockdown was significantly improved ( $P < 0.05$ ; Fig. 3C). Furthermore, the anti-angiogenic effects were shown *in vivo* by anti-CD31 immunohistochemistry following injection of miR-126 mimics or Camsap1 knockdown into tumors ( $P < 0.05$ ; Fig. 3D).



Figure 5. An evolutionary tree of Camsap1 generated by maximum likelihood analysis.

*The antitumor mechanism of miR-126 mimics or Camsap1 knockdown in LSCC cells.* To clarify the mechanism of miR-126 or Camsap1 in LSCC cells, TargetScan were used to determine whether Camsap1 is a target gene of miR-126 or not. The prediction results are shown in Fig. 4A. Furthermore, microtubules formed bundles and aggregated together in untreated cells by using negative stain electron microscopy (Fig. 4B). After knockdown treatment of miR-126 mimics or Camsap1, microtubules did not form such aggregates in LSCC cells. These results indicated Camsap1 induced the formation of bundles by directly interacting with microtubules (Fig. 4B). Interestingly, we demonstrated that Camsap1 and tubulin colocalized in the cytoplasm by using immunofluorescence (IF) (Fig. 4C).

*Phylogeny of the CAMSAP1 family.* To further study the functions of CAMSAP1 protein, we made use of it in a phylogenetic analysis of the family. Fig. 5 shows a tree generated by maximum likelihood analysis of a codon-based alignment. It appears that a CAMSAP1 gene arose in the ancestors of simple animals. During the evolution of the vertebrates, this gene was multiplied so that extant vertebrate genomes encode three classes of CAMSAP1 genes. These results indicated that we could get more information on CAMSAP1 gene from adjacent species, such as Gorilla.

## Discussion

Loss of miR-126 has been observed in many cancers, such as breast cancer (8), lung cancer (10) and prostate cancer (17). The decreased expression of miR-126 was associated with poor metastasis-free survival of breast cancer patients (18). In this study, we detected the level of miR-126 in plasma of the patients with LSCC. We also found loss of miR-126 was related with poor prognosis of the patients with LSCC. Similarly, the relationship between low miR-126 expression and worse disease prognosis has been reported in glioblastoma (19), and gastric cancer patients (20). Contrary to our results, Donnem *et al* (10) demonstrated that high miR-126 expression in tumor samples correlates with a shorter survival of NSCLC patients. Recent studies indicated that

circulating miRNA may become valuable biomarkers for different diseases. Long *et al* (21) found that circulating miR-126 might be useful biomarkers for ischemic stroke in humans. In this study, we confirmed that the plasma miR-126 could predict the survival rate of the patients with LSCC. Furthermore, we found the plasma level of miR-126 was also negatively related with Camsap1 expression. Based on this result, we hypothesized Camsap1 may be a target gene of miR-126.

CAMSAP1 is a protein expressed in the nervous system of mammals in neurons and astrocytes (22). CAMSAP1 contains a C-terminal CKK domain which binds microtubules, and was overexpressed in the model cell line PC12 (23). In this study, we also found that microtubules did not form aggregates in LSCC cells after miR-126 mimics or Camsap1 knockdown treatment. Interestingly, we confirmed Camsap1 and tubulin colocalized in the cytoplasm by using immunofluorescence. We constructed the evolutionary tree of Camsap1 by using phylogenetic analysis. In our study, we confirmed Camsap1 expression is higher in cancer tissues than normal tissues and its expression is related with the prognosis of the patients with LSCC. However, previous studies on Camsap1 are very scarce. We are not able yet to provide the exact mechanism of Camsap1 in LSCC, thus, further study is required.

In conclusion, we found miR-126 was able to inhibit LSCC partly by suppressing Camsap1 expression. Camsap1 expression induced microtubule formation and aggregation. The reported mechanism possibly explains why loss of miR-126 is frequently associated with tumor metastasis.

## Acknowledgements

This study was supported by the Grants from National Natural Science Foundation of China (no. 82072196).

## References

1. Du T and Zamore PD: microPrimer: the biogenesis and function of microRNA. *Development* 132: 4645-4652, 2005.
2. Chang TC and Mendell JT: microRNAs in vertebrate physiology and human disease. *Annu Rev Genomics Hum Genet* 8: 215-239, 2007.

3. Latronico MV, Catalucci D and Condorelli G: Emerging role of microRNAs in cardiovascular biology. *Circ Res* 101: 1225-1236, 2007.
4. Fish JE, Santoro MM, Morton SU, *et al*: miR-126 regulates angiogenic signaling and vascular integrity. *Dev Cell* 15: 272-284, 2008.
5. Wang S, Aurora AB, Johnson BA, *et al*: The endothelial-specific microRNA miR-126 governs vascular integrity and angiogenesis. *Dev Cell* 15: 261-271, 2008.
6. Feng R, Chen X, Yu Y, *et al*: miR-126 functions as a tumour suppressor in human gastric cancer. *Cancer Lett* 298: 50-63, 2010.
7. Liu B, Peng XC, Zheng XL, Wang J and Qin YW: MiR-126 restoration down-regulate VEGF and inhibit the growth of lung cancer cell lines in vitro and in vivo. *Lung Cancer* 66: 169-175, 2009.
8. Zhu N, Zhang D, Xie H, *et al*: Endothelial-specific intron-derived miR-126 is down-regulated in human breast cancer and targets both VEGFA and PIK3R2. *Mol Cell Biochem* 351: 157-164, 2011.
9. Slaby O, Redova M, Poprach A, *et al*: Identification of MicroRNAs associated with early relapse after nephrectomy in renal cell carcinoma patients. *Genes Chromosomes Cancer* 51: 707-716, 2012.
10. Donnem T, Fenton CG, Lonvik K, *et al*: MicroRNA signatures in tumor tissue related to angiogenesis in non-small cell lung cancer. *PLoS One* 7: e29671, 2012.
11. D'Alessandra Y, Devanna P, Limana F, *et al*: Circulating microRNAs are new and sensitive biomarkers of myocardial infarction. *Eur Heart J* 31: 2765-2773, 2010.
12. Su X, Chakravarti D, Cho MS, *et al*: TAp63 suppresses metastasis through coordinate regulation of Dicer and miRNAs. *Nature* 467: 986-990, 2010.
13. Watahiki A, Macfarlane RJ, Gleave ME, *et al*: Plasma miRNAs as biomarkers to identify patients with castration-resistant metastatic prostate cancer. *Int J Mol Sci* 14: 7757-7770, 2013.
14. Jung EJ, Santarpia L, Kim J, *et al*: Plasma microRNA-210 levels correlate with sensitivity to trastuzumab and tumor presence in breast cancer patients. *Cancer* 118: 2603-2614, 2012.
15. Ivkovic-Kapic T, Knelevic-Usaj S, Panjkovic M and Mastilovic K: Immunohistochemical analysis of angiogenesis in invasive ductal breast carcinoma with correlations to clinicopathological factor. *Vojnosanit Pregl* 63: 635-642, 2006.
16. Lewis BP, Burge CB and Bartel DP: Conserved seed pairing, often flanked by adenosines, indicates that thousands of human genes are microRNA targets. *Cell* 120: 15-20, 2005.
17. Sun X, Liu Z, Yang Z, *et al*: Association of microRNA-126 expression with clinicopathological features and the risk of biochemical recurrence in prostate cancer patients undergoing radical prostatectomy. *Diagn Pathol* 8: 208, 2013.
18. Zhang Y, Yang P, Sun T, *et al*: miR-126 and miR-126\* repress recruitment of mesenchymal stem cells and inflammatory monocytes to inhibit breast cancer metastasis. *Nat Cell Biol* 15: 284-294, 2013.
19. Feng J, Kim ST, Liu W, *et al*: An integrated analysis of germline and somatic, genetic and epigenetic alterations at 9p21.3 in glioblastoma. *Cancer* 118: 232-240, 2012.
20. Li X, Zhang Y, Zhang Y, *et al*: Survival prediction of gastric cancer by a seven-microRNA signature. *Gut* 59: 579-585, 2009.
21. Long G, Wang F, Li H, *et al*: Circulating miR-30a, miR-126 and let-7b as biomarker for ischemic stroke in humans. *BMC Neurol* 13: 178, 2013.
22. Yamamoto M, Yoshimura K, Kitada M, *et al*: A new monoclonal antibody, A3B10, specific for astrocyte-lineage cells recognizes calmodulin-regulated spectrin-associated protein 1 (Camsap1). *J Neurosci Res* 87: 503513, 2009.
23. Baines AJ, Bignone PA, King MD, *et al*: The CKK domain (DUF1781) binds microtubules and defines the CAMSAP/ssp4 family of animal proteins. *Mol Biol Evol* 26: 2005-2014, 2009.